Mechanical Property Evaluation of Hybrid Mixed-Species CLT Panels with Sugar Maple and White Spruce

Yunxiang Ma, S.M.ASCE[1]; Ruizhe Si[2]; Munkaila Musah[3]; Qingli Dai, M.ASCE[4]; Xinfeng Xie[5]; Xiping Wang[6]; and Robert J. Ross[7]

Abstract: This study evaluated the mechanical properties of hybrid (mixed-species) cross-laminated timber (CLT) panels made of low-value sugar maple (*Acer saccharum*) and white spruce (*Picea glauca*). The modulus of elasticity (MOE) of the laminations was measured with a nondestructive method. Three-layer hybrid CLT panels with layup combinations of sugar maple–white spruce–sugar maple and white spruce–sugar maple–white spruce were prepared to evaluate the effects of layups on the performance of the CLT samples. The mechanical properties of hybrid CLT panels were evaluated with different layups and both melamine- and resorcinol-based adhesives. Both long-span and short-span third-point bending tests were conducted to study the flexural and shear behavior of each CLT panel type. It was found that the influence of adhesive types was not significant. The mechanical properties of the hybrid CLT panels with sugar maple surface layers were improved significantly compared with those of the current standard layups. Both bending tests were simulated with finite-element analysis based on measured and reference material properties. The simulated results of each case were in good agreement with the test results. **DOI: 10.1061/(ASCE)MT.1943-5533.0003760.**

Author keywords: Cross-laminated timber (CLT); Mixed species; Low-value hardwood; Flexural properties; Finite-element modeling.

Introduction

As an innovative timber panel product, cross-laminated-timber (CLT) expands the structural utilization of mass timber into two-dimensional components with its orthogonal flatwise and edgewise behavior. The cross-laminated layup reduces the property variance caused by local defects such as checks, knots, and wane by redistributing the loads into other directions (Brandner 2013). Standards and design guides such as APA PRG-320 (APA 2019) and the CLT handbook (Karacabeyli and Douglas 2013) allow industrial applications of CLT panels. However, current regulations provide several layup designs only with spruce-pine-fir (SPF) or engineered wood products such as laminated veneer lumber (LVL), laminated strand lumber (LSL), and oriented strand lumber (OSL). Expanding the source of timber by including more wood species in CLT manufacturing has been a main interest in the study of CLT manufacturing (Sun et al. 2020). Unlike traditional CLT, hybrid CLT has a hybrid layup with multiple species of different grades. Applying a layer with stronger species in the CLT layup can enhanced the mechanical properties of the CLT.

Some studies have explored the use of multiple softwood species in CLT fabrication. However, studies of CLT with a combination of softwood and hardwood are very limited. Wang et al. (2014) investigated the use of poplar as the cross-layer in CLT fabrication and tested different types of CLT panel samples, including pure poplar (*Populus euramericana*), pure Monterey pine (*Pinus radiata D. Don*), pure Douglas fir (*Pseudotsuga menziesii*), and the two mixed-species layups with Monterey pine or Douglas fir surface layers and a poplar cross-layer. The results indicated that poplar could be used in CLT fabrication, and provided similar mechanical properties to common softwood CLT. Similarly, CLT panels made with Douglas fir and poplar layers were studied by Lu et al. (2019). The panels were tested in third-point bending tests for flexural performance. Strain gauges were used to study the strain distribution at the midspan. The results showed that hybrid panels made with Douglas fir and poplar could provide sufficient mechanical performance. It was also concluded that the Douglas fir–poplar mixed layup can improve the performance of CLT compared with pure poplar CLT panels.

Because sugar maple is much stronger than poplar, it can be expected that the utilization of low-value sugar maple could improve the mechanical performance of CLT comparing with standard softwood CLT. Hardwood with grade equal to or lower

[1]Graduate Research Assistant, Dept. of Civil and Environmental Engineering, Michigan Technological Univ., 1400 Townsend Dr., Houghton, MI 49931. Email: yma2@mtu.edu

[2]Research Associate, Institute of Civil Engineering Materials, School of Civil Engineering, Southwest Jiaotong Univ., Chengdu 610031, China. Email: ruizhesi@swjtu.edu.cn

[3]Graduate Research Assistant, College of Forest Resources and Environmental Science, Michigan Technological Univ., 1400 Townsend Dr., Houghton, MI 49931. ORCID: https://orcid.org/0000-0003-1690-6264. Email: mmusah@mtu.edu

[4]Professor, Dept. of Civil and Environmental Engineering, Michigan Technological Univ., 1400 Townsend Dr., Houghton, MI 49931 (corresponding author). ORCID: https://orcid.org/0000-0001-7760-8012. Email: qingdai@mtu.edu

[5]Assistant Professor, College of Forest Resources and Environmental Science, Michigan Technological Univ., 1400 Townsend Dr., Houghton, MI 49931. ORCID: https://orcid.org/0000-0002-6478-9827. Email: xinfengx@mtu.edu

[6]Research Forest Products Technologist, USDA Forest Service, Forest Products Laboratory, 1 Gifford Pinchot Dr., Madison, WI 53726; Research Professor, College of Forest Resources and Environmental Science, Michigan Technological Univ., 1400 Townsend Dr., Houghton, MI 49931. Email: xiping.wang@usda.gov

[7]Acting Assistant Director, USDA Forest Service, Forest Products Laboratory, 1 Gifford Pinchot Dr., Madison, WI 53726; Research Professor, College of Forest Resources and Environmental Science, Michigan Technological Univ. Email: robert.j.ross@usda.gov

Note. This manuscript was submitted on July 19, 2020; approved on November 18, 2020; published online on May 5, 2021. Discussion period open until October 5, 2021; separate discussions must be submitted for individual papers. This paper is part of the ***Journal of Materials in Civil Engineering***, © ASCE, ISSN 0899-1561.

than #1 common according to the NHLA standard are usually considered to be low-value hardwood, which is difficult to use in furniture and flooring manufacture (NHLA 2019). Low-value hardwoods are used mostly in the manufacture of paper, pallet, railroad ties, and so forth (Thomas and Buehlmann 2017), which are low-value-added products. In the Great Lake region, interest in using low-value sugar maple (*Acer saccharum* Marsh) in high-value-added CLT is increasing. This new utilization option could provide a more valuable product market in the region, which is expected to motivate forest management further and result in a positive environmental impact.

The bending strength (MOR) and bending elastic modulus (MOE), shear modulus (G), and shear strength are the major mechanical properties used to evaluate the structural performance of CLT. Current standards ASTM D198 (ASTM 2015) and PRG 320 (APA 2019) recommend evaluating the flexural properties with the long-span third-point bending test. The recommended span-to-depth ratio is about 30, to limit the shear effects. CLT made with Canadian hemlock was tested with a span of 27.85 times the depth for the flexural performance by He et al. (2018). Hindman and Bouldin (2015) used a span-to-depth ratio of 27:1 for CLT samples. According to ASTM D198 (ASTM 2015) and PRG 320 (APA 2019), a span-to-depth ratio of 4–6 is recommended to determine the shear properties of CLT panels. The shear properties of CLT panels were studied via experimental and simulated short-span flexural tests by Flores et al. (2016). Both long-span and short-span bending tests were conducted to thoroughly evaluate the mechanical properties of a new CLT product (Navaratnam et al. 2020). They also were used as the main approach to evaluate the mechanical properties of CLT to investigate the influence of manufacturing parameters (Sharifnia and Hindman 2017). The present study conducted long-span and short-span bending tests to evaluate the bending and shear properties of hybrid CLT beams.

As an efficient and viable tool, finite-element (FE) simulation has been applied to estimate the mechanical properties and performance of the CLT panels. He et al. (2018) investigated the bending and compressive properties of CLT made with Canadian hemlock with integrated experimental and numerical analysis. The results indicated that the FE models could simulate the hemlock CLT panels in bending. Similarly, Chen and Lam (2012) investigated complex layups with different interlayer angles using experimental and numerical methods. They reported that the behavior of a combined timber structure system could be estimated with FE models. FE models also can capture the damage behavior of timber with Hashin damage criteria (Hashin and Rotem 1973). The constitutive law was established to model arbitrarily orientated timber with a failure criteria based on the Hashin damage model (Gharib et al. 2017). It has been validated with experimental data and proved adequate. For ribbed CLT plates, which are more complex structures, the design also can be optimized with the Hashin damage criteria (Brank et al. 2017). The Hashin damage criteria is capable of capturing the orthogonal distribution of the timber capacity, and therefore was applied in this study.

The primary objective of this study was to evaluate the mechanical properties of the developed hybrid CLT panels with low-value sugar maple (*Acer saccharum*) and white spruce (*Picea glauca*) boards through mechanical tests and numerical simulation. First, the general manufacturing procedure of the CLT samples is presented. The correlated long-span and short-span bending tests then are presented with the method and results. The modeling procedures and parameter definition of the orthogonal material model and damage model are summarized for the simulation of both tests. The simulation results are discussed, which show that the model is capable of adequately estimating CLT panel bending and shear properties.

CLT Sample Preparation

Preparation of Laminations

White spruce and sugar maple boards were prepared as the laminations of hybrid CLT panels. The thickness of the boards was 22.9 mm for sugar maple and 36.8 mm for white spruce, whereas the length of both types of boards was 2.44 m. The modulus of elasticity (MOE) of each individual lamination was determined using a nondestructive transverse vibration method based on ASTM D6874 (ASTM 2012). Following a vertical impact at the midspan, the free vibration of each board was captured and recorded by a data acquisition system. The weight of the board was measured by the load cell. With the inputs of the dimensions and weight of each lumber, the bending modulus was calculated using

$$\mathrm{MOE}_{\mathrm{ND}} = \frac{WL^3 f^3}{Kbh^3} \tag{1}$$

where h, b, and L = depth, width, and length of board, respectively; W = weight; f = vibration frequency; and K is a calibration constant, which was calibrated with a reference aluminum bar before testing. The moisture content (MC) was controlled between 8% and 12% during the procedure.

The low-value sugar maple had an average MOE of 14,230 MPa, and the coefficient of variation (COV) of 31.7% (Musah 2020). The white spruce used in this study had an average MOE of 9,225 MPa, with a coefficient of variation of 5.87%.

CLT Panel Manufacture and Sample Preparation

A total of nine three-layer CLT panels were manufactured from the tested boards with three types of layup and adhesive combinations: (1) sugar maple–white spruce–sugar maple (HSH) layup glued with melamine-formaldehyde (M); (2) sugar maple–white spruce–sugar maple (HSH) layup glued with resorcinol-formaldehyde (R); and (3) white spruce–sugar maple–white spruce (SHS) layup glued with resorcinol formaldehyde (R) adhesive. The CLT panels were made and cured with a hydraulic press, and the dimensions were 610 mm wide and 2.44 m long. The thickness of HSH panels was 82.6 mm, and the thickness of the SHS samples was 96.5 mm.

Boards were maintained in a conditioning chamber to keep the MC at about 12%. Board edges were planed and side-glued with Titebond (Columbus, Ohio) using clamps. They were kept under clamping pressure for 24 h. Due to the maximum width limit of the planer, the boards were initially glued into subsections within each layer so that they could be surfaced using the planer. Subsections were three and four boards wide for the outer parallel layers, and four or five boards wide for the middle perpendicular layer. After the boards were edge-glued into subsections, they were surface planed, and the subsections were side-glued to form the full layer. Within 24 h of this surface planing, the layers were surface glued. The core layers were placed in a room with the temperature set at 27°C (81°F) for 1–2 h to bring the board temperature to 70°F prior to applying the adhesive. The adhesive application rate was 0.472 kg (1.04 lb) of adhesive for each bonding interface. Then the layers were stacked and pressed under pressure of 0.8 MPa at about 75°F for 4 h.

Each type of CLT had three sample panels. From each panel, a long CLT beam sample (L) was prepared for the long-span flexural test, and two short CLT beam samples (S) were prepared for the short-span flexural test. In total, 9 long beam samples and 18 short beam samples were prepared. The long beam sample was 305 mm wide and 2.44 m long, whereas the short beam sample was 254 mm wide and 457 mm long. All CLT samples were coded to reflect the type of layups (HSH or SHS), the adhesive used (M or R), and the

Table 1. Average MOE of laminations in each layer and each CLT sample (MPa)

CLT panel code	MOE of longitudinal layers		MOE of transverse layer	Longitudinal layers average MOE	Transverse layer average MOE
	Top layer	Bottom layer	Middle layer		
M-HSH-(L1, S1–2)	1.52×10^4	1.80×10^4	8.56×10^3	1.66×10^4	7.72×10^3
M-HSH-(L2, S3–4)	1.61×10^4	1.70×10^4	7.21×10^3		
M-HSH-(L3, S5–6)	1.67×10^4	1.67×10^4	7.39×10^3		
R-HSH-(L1, S1–2)	1.67×10^4	1.62×10^4	8.15×10^3	1.67×10^4	9.30×10^3
R-HSH-(L2, S3–4)	1.77×10^4	1.68×10^4	1.05×10^4		
R-HSH-(L3, S5–6)	1.61×10^4	1.69×10^4	9.26×10^3		
R-SHS-(L1, S1–2)	8.29×10^3	1.03×10^4	1.74×10^4	9.73×10^3	1.52×10^4
R-SHS-(L2, S3–4)	9.00×10^3	1.72×10^4	1.02×10^4		
R-SHS-(L3, S5–6)	9.59×10^3	1.09×10^4	1.10×10^4		

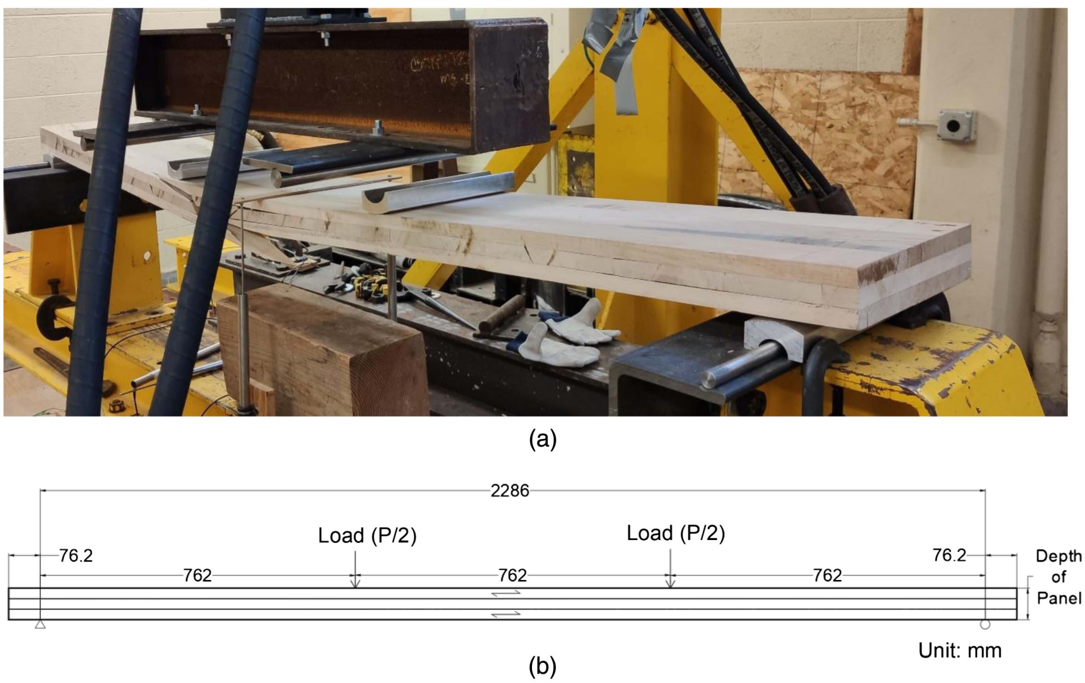

Fig. 1. Long-span bending test setup: (a) loading frame and fixtures; and (b) dimensions of the long-span sample.

test conducted (L or S). Table 1 lists the code of each sample, the average MOE of the laminations used in each layer, and the average MOE of each CLT panel.

Experimental Evaluation

Two static bending tests were conducted to evaluate the bending and shear performance of the designed CLT panels manufactured with the combinations of sugar maple and spruce. Long-span and short-span beam samples were cut from each type of CLT panels and used for bending and shear performance evaluation, respectively.

Test and Calculation Methods

Block Shear Test

Block shear tests were conducted according to ASTM D905 (ASTM 2013) with 25 samples of 8 replicates. A total of 400 shear blocks were tested, and 250 delamination blocks of 10 replicates were tested. The testing was conducted at a loading rate of 2 mm/min in a universal testing machine with 1,000-kN (225-kips) capacity. Specimens were prepared according to the ANSI PRG 320 (APA 2019) standard based on the ASTM D905 (ASTM 2013). Wood failure was estimated immediately after the block shear test in accordance with ASTM D5266 (ASTM 2011).

Long-Span Bending Test

The third-point bending test was conducted on the long-span samples to evaluate the bending performance of the manufactured CLT panels. The test was conducted in accordance with ASTM D198 (ASTM 2015). The span of the tested samples was fixed at 2.29 m (90 in.) to ensure a span-to-depth ratio above 20, which limited the shear effect during the long-span bending test. A loading rate of 10 mm/min (0.4 in./min) was used for the test. In accordance with the recommendation of the ASTM D198 standard (ASTM 2015), the total testing time was approximately 10 min. The scheme for the loading frame and the fixtures of the long-span bending test are shown in Fig. 1.

Because the span-to-depth ratio of the long-span samples was large, the shear effect was negligible (Karacabeyli and Douglas 2013). The modulus of elasticity of the CLT beam (MOE_{CLT}) can be obtained as

$$MOE_{CLT} = \frac{Pa}{2\Delta_{max} I}\left(\frac{l^2}{8} - \frac{a^2}{6}\right) \quad (2)$$

where P = peak load, a = distance from center of support to nearest loading location; Δ_{max} = maximum displacement of beam during test; l = beam span; and I = moment of inertia of CLT beam.

When the sample reached the peak load, the modulus of rupture of the CLT beam (MOR_{CLT}) was defined as

$$MOR_{CLT} = \frac{P \cdot a \cdot y}{2 \cdot I} \quad (3)$$

where y = distance of beam bottom to neutral axis, which was half the total depth.

Short-Span Bending Test (Third-Point Bending Test)

The center-point bending test was conducted on the short-span beam samples to evaluate the shear performance of the hybrid CLT panels. The test was conducted in accordance with ASTM D198 (ASTM 2015). The thickness of the M-HSH-L and R-HSH-L samples was 82.55 mm, and the thickness of the R-SHS-L samples was 96.52 mm. The span of the tested samples was fixed at 381 mm. A loading rate of 10 mm/min (0.4 in./min) was used for the test according to the recommendation of ASTM D198 (ASTM 2015). Detailed information for the loading frame and the fixtures of the center-point bending test is shown in Fig. 2.

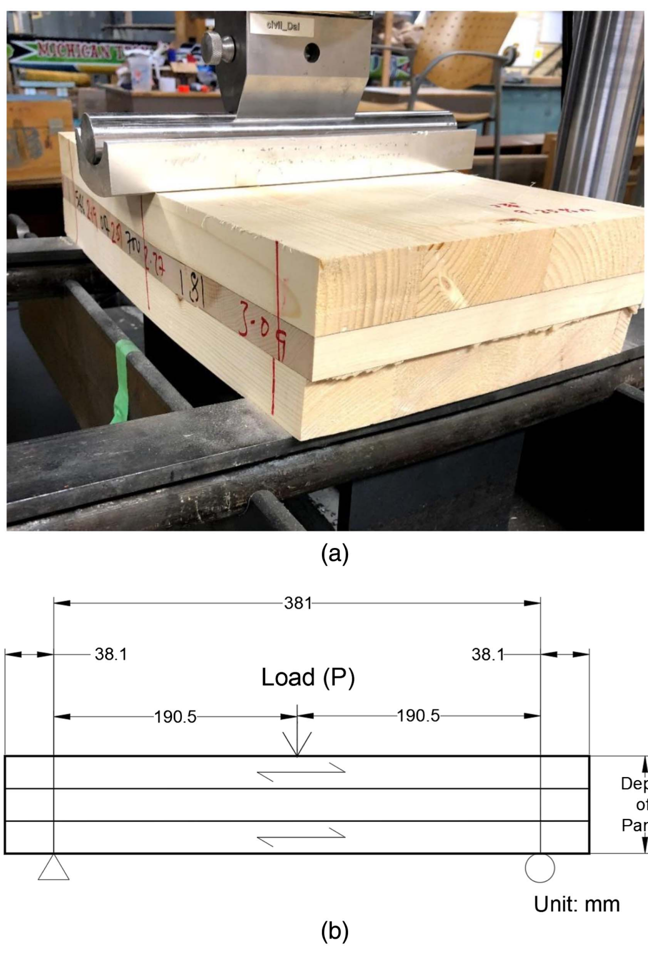

Fig. 2. Short-span bending test setup: (a) loading frame and fixtures; and (b) dimensions of the short-span CLT beam sample.

For the short-span samples, the shear performance was the major expected outcome. According to the shear analogy method, which is the primary design method in the US CLT handbook (Karacabeyli and Douglas 2013), the shear stiffness can be calculated as

$$GA_{\text{eff-test}-S} = \frac{K_s EI_{\text{eff}}}{\left(\frac{EI_{\text{eff}}}{EI_{\text{app-test}-S}} - 1\right) l^2} \quad (4)$$

where K_s = shear influence factor, which is 14.4 for three-point bending with pinned ends; EI_{eff} = effective bending stiffness calculated using shear analogy method; and $EI_{\text{app-test}-S}$ = apparent bending stiffness from short-span tests that include the contribution of the shear effect. The effective bending stiffness EI_{eff} is calculated as

$$EI_{\text{eff}} = \sum_{i=1}^{n} E_i b_i h_i^3/12 + \sum_{i=1}^{n} E_i A_i z_i^2 \quad (5)$$

It is calculated with the elastic modulus of each layer in the panel longitudinal direction (E_i), depth (h_i), and the distance between the layer neutral axis and the panel neutral axis (z_i). The width (b_i) is set as unit length, and the area (A_i) is calculated accordingly.

The equivalent shear modulus (G) of the short-span panels can be calculated as

$$G_{\text{eq}} = GA_{\text{eff-test}-S}/A \quad (6)$$

The panel reaches the shear strength when the load reaches the peak value (P). The shear strength is not distributed evenly due to the different directions of the layers. As a result, the shear strength need to be presented as equivalent shear strength in order to compare panels with different cross depths. The equivalent shear strength can be calculated as

$$f_{s,\text{eq}} = \frac{V}{A} = \frac{P}{2 \cdot A} \quad (7)$$

Test Results

Block Shear Test Results

The results of block shear test are shown in Fig. 3. The average wood failure percentage was more than 90% for all three types

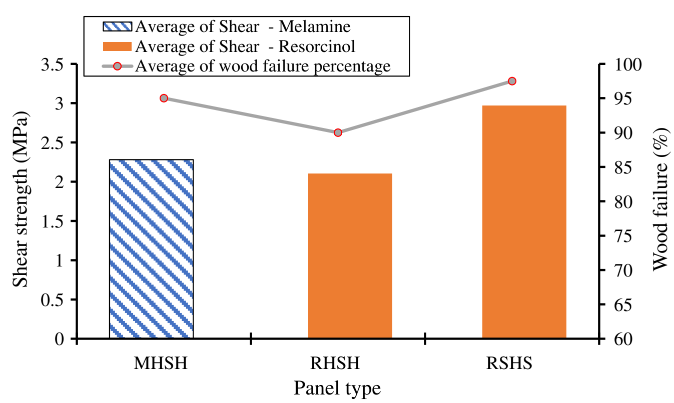

Fig. 3. Test results of block shear test.

Table 2. MOE_{CLT} and MOR_{CLT} results of long-span bending test of three sample types

CLT panels	MOE (GPa)	Average MOE (GPa)	MOE coefficient of variation (%)	MOR (MPa)	Average MOR (MPa)	MOR coefficient of variation (%)
M-HSH-L1	28.9	23.9	20.6	36.2	43.9	12.4
M-HSH-L2	25.7			47.9		
M-HSH-L3	17.2			47.7		
R-HSH-L1	24.4	22.6	6.7	39.2	46.2	39.2
R-HSH-L2	20.7			48.2		
R-HSH-L3	22.8			81.3		
R-SHS-L1	18.4	16.3	21.5	50.8	43.7	22.3
R-SHS-L2	19.2			50.3		
R-SHS-L3	11.4			29.9		

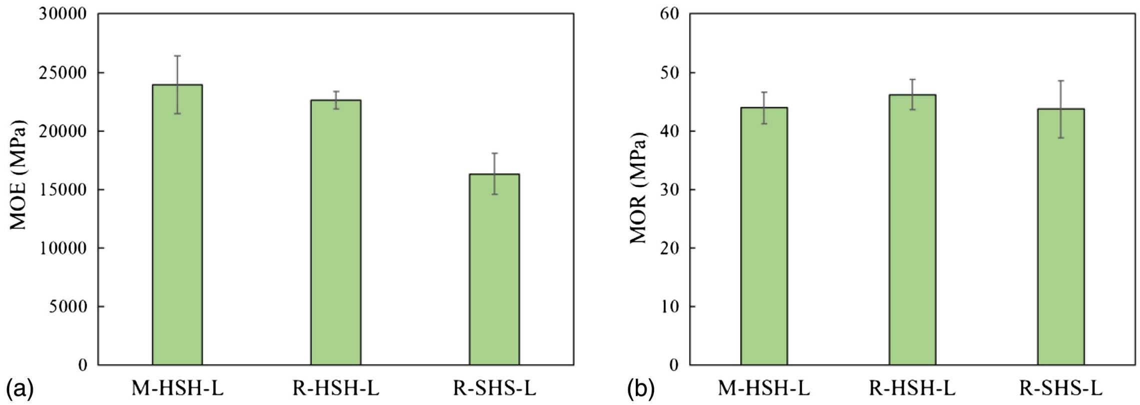

Fig. 4. Manufactured long-span CLT panels: (a) MOE; and (b) MOR.

of sample. The direct shear strength of the bonding surface was at least 2 MPa. The shear strength of bonded interfaces in RHSH samples was slightly lower than in RSHS samples, which indicates that the gluing and manufacture of the RHSH sample were not as good as those of the RSHS samples. However, the bonding was adequate for all three types of samples.

Bending Properties of Hybrid CLT Panels

The results of the third-point bending test for long-span CLT beams are given in Table 2 and Fig. 4. The MOE_{CLT} of the M-HSH-L, R-HSH-L, and R-SHS-L beams was 23.94, 22.63, and 16.32 GPa, respectively. Comparing the M-HSH-L and R-HSH-L samples, it was found that the MOE of the HSH CLT beams manufactured with different adhesives was relatively close (23.94 versus 22.63 GPa). However, comparing different layups, the MOE of R-SHS-L was 27.9% less than that of R-HSH-L [Fig. 4(a)]. The bending strength of the long-span CLT panels (i.e., MOR_{CLT}) had a different trend than the MOE of the long-span CLT panels. The MOR_{CLT} of the R-HSH-L samples was approximately the same as that of the M-HSH-L samples [Fig. 4(b)]. In terms of different layups, unlike the trend of MOE_{CLT}, the MOR_{CLT} of R-SHS-L had no significant reduction compared with that of R-HSH-L. This could be the result of the different failure mode. The R-SHS-L samples had more bending failure (bottom splinter), whereas most of the failures of R-HSH-L were initiated by shear damage. The different weaknesses provided similar overall load capacity. The coefficient of variation of the measured MOE and MOR was 6.7%–39.2% (Table 2). Due to the high variance of timber material, the results may not be adequate to provide specific quantitively correlations.

Effects of Adhesives and Layups on Bending Performance of Hybrid CLT Panels

Comparison of the average values indicated that the MOE of the long-span beams was not significantly affected by the type of adhesives [Fig. 4(a)]. The average MOR of the R-HSH-L was similar to that of the M-HSH-L, which indicates that the adhesive type did not affect the MOR. The results showed that the layups of the CLT panels had more influence on the MOE_{CLT} of the panels than on the failure strength of the samples. Because the spruce possessed a lower MOE than the sugar maple, the R-SHS-L with two weaker layers (spruce) tended to have a lower overall MOE than that of R-HSH-L. Hence, the MOE of R-SHS-L was less than that of R-HSH-L.

Comparing Bending Performance of Hybrid CLT Panels with Reference Values in APA/PRG-320

The standard for performance-rated cross-laminated timber, ANSI/APA PRG 320 (APA 2019), provided the reference properties for the CLT panels. Layup E1 is composed of two layers of 1950f-1.7E spruce-pine-fir lumber as outer layers and one layer of No. 3 spruce-pine-fir lumber as a middle layer. The MOE_{CLT} of the CLT panels with the combination of the spruce and sugar maple generally was higher than that of E1-grade CLT defined in ANSI/APA PRG 320 (APA 2019) [Fig. 5(a)]. Notably, the MOE_{CLT} of the M-HSH-L and the R-HSH-L improved by 111% and 100% compared with that of E1-grade CLT. In addition, the designed spruce–maple CLT panels had 30%–120% greater MOR than E1-grade CLT [Fig. 5(b)].

Shear Performance of Hybrid CLT Panels

The shear performance of the hybrid CLT panels was evaluated based on the center-point bending test of short-span CLT panels.

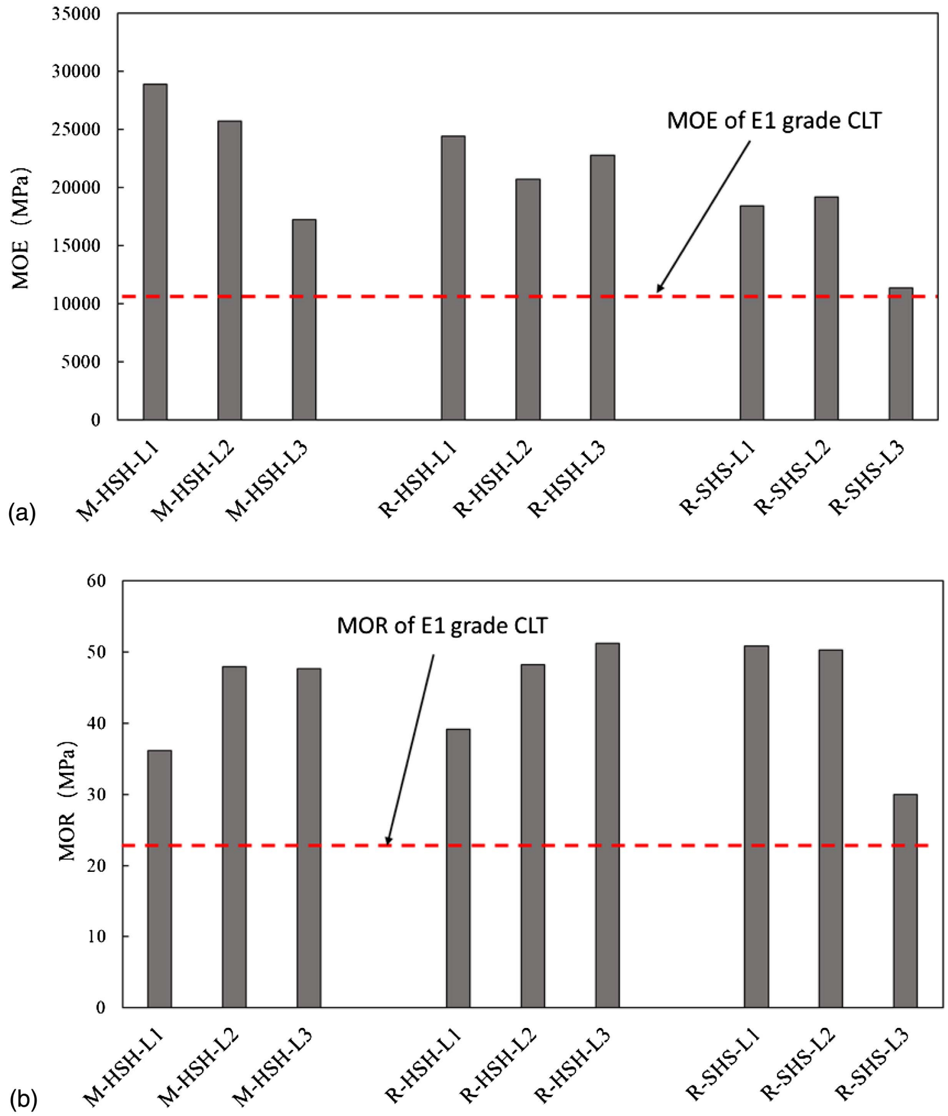

Fig. 5. Reference value in APA/PRG-320 (APA 2019) and measured value of (a) MOE; and (b) MOR.

The shear modulus and shear strength of the short-span tested CLT panels are given in Table 3 and Fig. 6. The shear modulus of the R-HSH-S was 7.8% less than that of M-HSH-S. The samples glued with melamine adhesive had better shear performance than samples glued with resorcinol. The shear modulus of the R-SHS-S samples was 43.3% less than that of the R-HSH-S samples [Table 3; Fig. 6(b)]. The equivalent shear strength of the M-HSH-S, R-HSH-S, and R-SHS-S samples was 1.81, 1.70, and 2.11 MPa, respectively. The results showed that the shear strength of the hybrid CLT panels in this study was not significantly affected by the adhesive type. However, in terms of different layups, unlike the trend of shear modulus, the R-SHS-S samples had a higher equivalent shear strength than the R-HSH-S sample. Because of the weaker shear strength of the transverse layer due to the lamination direction, the middle layer(s) tend to be more vulnerable under shear. Therefore, it is logical that a stronger transverse layer enhanced the shear strength of the panel. According to the shear analogy method, the shear modulus of the panel depends more on the top and bottom layers. As a result, the shear modulus of the SHS layup was less than that of the HSH layup, whereas the shear strength was enhanced. Similar to the long-span test, the variation of the short-span test result was about 10%–20%. It could be reduced by applying more replicates. Nevertheless, the results did provide a clear trend though the high variation limited the reduction.

Comparing Shear Performance of Hybrid CLT Panels with Reference Values in APA/PRG-320

The shear performance of the designed spruce–sugar maple CLT panels obtained from the short-span bending test of the samples was compared with the reference shear modulus of the E1-grade CLT panel in ANSI/APA PRG 320 (APA 2019) (Fig. 7). M-HSH-S and R-HSHS-S samples with two maple layers generally had a similar modulus as the E1-grade CLT [Fig. 7(a)]. Most of the tested shear moduli of the R-SHS-S samples were about half that of the E1-grade CLT panel. In addition, the shear strength of the designed CLT panels significantly increased (at least 280%) compared with that of the E1-grade CLT panel [Fig. 7(b)]. In summary, the MOE_{PL}, MOR_{PL}, shear modulus, and shear strength of the designed spruce–sugar maple CLT panels generally can fulfill the mechanical property requirements of the E1-grade CLT panel defined in ANSI/APA PRG 320 (APA 2019, 2011).

Table 3. Shear modulus (G) and equivalent shear strength ($f_{s,\mathrm{eq}}$) results of short-span bending test of three sample types

Sample type	G (MPa)	Average G (MPa)	G COV (%)	Equivalent shear strength (MPa)	Average equivalent shear strength (MPa)	Equivalent shear strength CoV (%)
M-HSH-S1	65.47	58.40	19.7	2.35	1.81	13.8
M-HSH-S2	57.98			1.77		
M-HSH-S3	43.51			1.7		
M-HSH-S4	70.79			1.77		
M-HSH-S5	69.76			1.57		
M-HSH-S6	42.89			1.7		
R-HSH-S1	53.85	60.30	17.8	1.3	1.7	22.3
R-HSH-S2	67.01			1.29		
R-HSH-S3	40.72			2.36		
R-HSH-S4	74.44			1.6		
R-HSH-S5	65.14			1.64		
R-HSH-S6	60.67			1.99		
R-SHS-S1	44.70	35.27	16.6	2.42	2.11	24.7
R-SHS-S2	30.28			3.1		
R-SHS-S3	37.87			2.05		
R-SHS-S4	26.98			1.72		
R-SHS-S5	33.18			1.61		
R-SHS-S6	38.62			1.73		

Computational Modeling and Simulation

The long-span test and the short-span test were simulated with finite-element software Abaqus version 2018 to provide an additional point of view on the panel bending and shear performance. The average value of the modulus and strengths were input for each CLT type by layer. The model parameters were assigned based on the global direction.

Material Model

The anisotropic behavior of the timber was modeled with an orthotropic elastic material model in the finite-element analysis platform Abaqus version 2018. The radial and tangential direction of each point in the lamination is highly dependent on the lumber preparation, which leads to a high variation and requirement of a polar coordinate system for each type of lumber. Modeling the laminations with the exact directions is possible, but it requires extensive extra measurement and model preparation. As a result, the local timber direction was simplified to be the same as the lamination coordinate system. As shown in Fig. 8, the longitudinal, tangential, and radial directions were assigned separately as the x-, y-, and z-directions of the lamination. A homogenous orthotropic elastic material model and a three-dimensional (3D) shell element were assigned for the models. The elastic compliance of the material was set as

$$\begin{bmatrix} 1/E_1 & -\nu_{21}/E_2 & -\nu_{31}/E_3 & 0 & 0 & 0 \\ -\nu_{12}/E_1 & 1/E_2 & -\nu_{32}/E_3 & 0 & 0 & 0 \\ -\nu_{13}/E_1 & -\nu_{23}/E_2 & 1/E_3 & 0 & 0 & 0 \\ 0 & 0 & 0 & 1/G_{12} & 0 & 0 \\ 0 & 0 & 0 & 0 & 1/G_{13} & 0 \\ 0 & 0 & 0 & 0 & 0 & 1/G_{23} \end{bmatrix} \begin{Bmatrix} \sigma_{11} \\ \sigma_{22} \\ \sigma_{33} \\ \sigma_{12} \\ \sigma_{13} \\ \sigma_{23} \end{Bmatrix} = \begin{Bmatrix} \varepsilon_{11} \\ \varepsilon_{22} \\ \varepsilon_{33} \\ \gamma_{12} \\ \gamma_{13} \\ \gamma_{23} \end{Bmatrix} \quad (8)$$

where ε_{ii} and γ_{ij} = strain in corresponding directions; E_i, ν_{ij}, and G_{ij} = elastic modulus, Poisson's ratio, and shear modulus, respectively, in each direction; σ_{ij} = corresponding stress; and subscripts 1, 2, and 3 denote lamination directions x, y, and z. Three elastic moduli E_1, E_2, and E_3; three shear moduli G_{12}, G_{13}, and G_{23}; and three Poisson's ratios ν_{12}, ν_{13}, and ν_{23} were input into the material model because the stiffness matrix was symmetrical ($\nu_{ij}/E_i = \nu_{ji}/E_j$).

The material property parameters were determined based on the nondestructive dynamic flexural test of the laminations. The elastic modulus of each layer was determined as the area average of all contained laminations based on the nondestructive modulus rating. For each layer, the modulus inputs were based on the tested lamination $\mathrm{MOE_{ND}}$ from Table 1 and the conversion ratios provided in *Wood Handbook* (Ross 2010) according to the species. The moisture content of all the lumbers was assumed to be constant at 12% during the simulation.

The conversion ratio of white spruce layers is not available in *Wood Handbook* (Ross 2010). Engelmann spruce is considered to be very close to white spruce (Khasa and Dancik 1996). Therefore, the conversion ratio data of Engelmann spruce were used to calculate the modulus of the white spruce layer. The elastic moduli in the tangential and radius directions were 0.059 and 0.128 times the longitudinal elastic modulus. The shear moduli in the longitudinal–radial (LR), longitudinal–tangential (LT), and tangential–radial (TR) directions were determined to be 0.124, 0.12, and 0.01 times the tested longitudinal $\mathrm{MOE_{ND}}$ (Ross 2010). The mean longitudinal MOE of white spruce has been tested as 9,642 MPa (Shivnaraine and Smith 1990), 6,214 MPa (Beaulieu et al. 2007), 7,954 MPa (Zhou and Smith 2007), and 9,852 MPa (Bendtsen 1974). In this

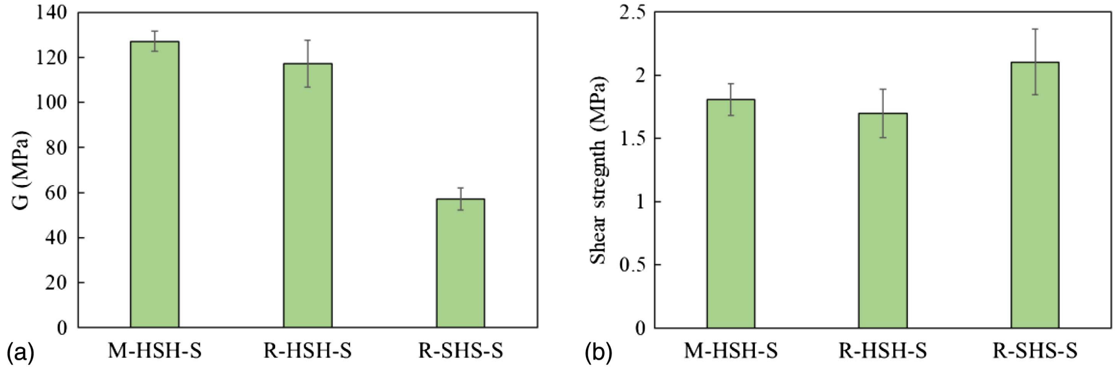

Fig. 6. Manufactured short-span CLT panels: (a) shear modulus; and (b) shear strength.

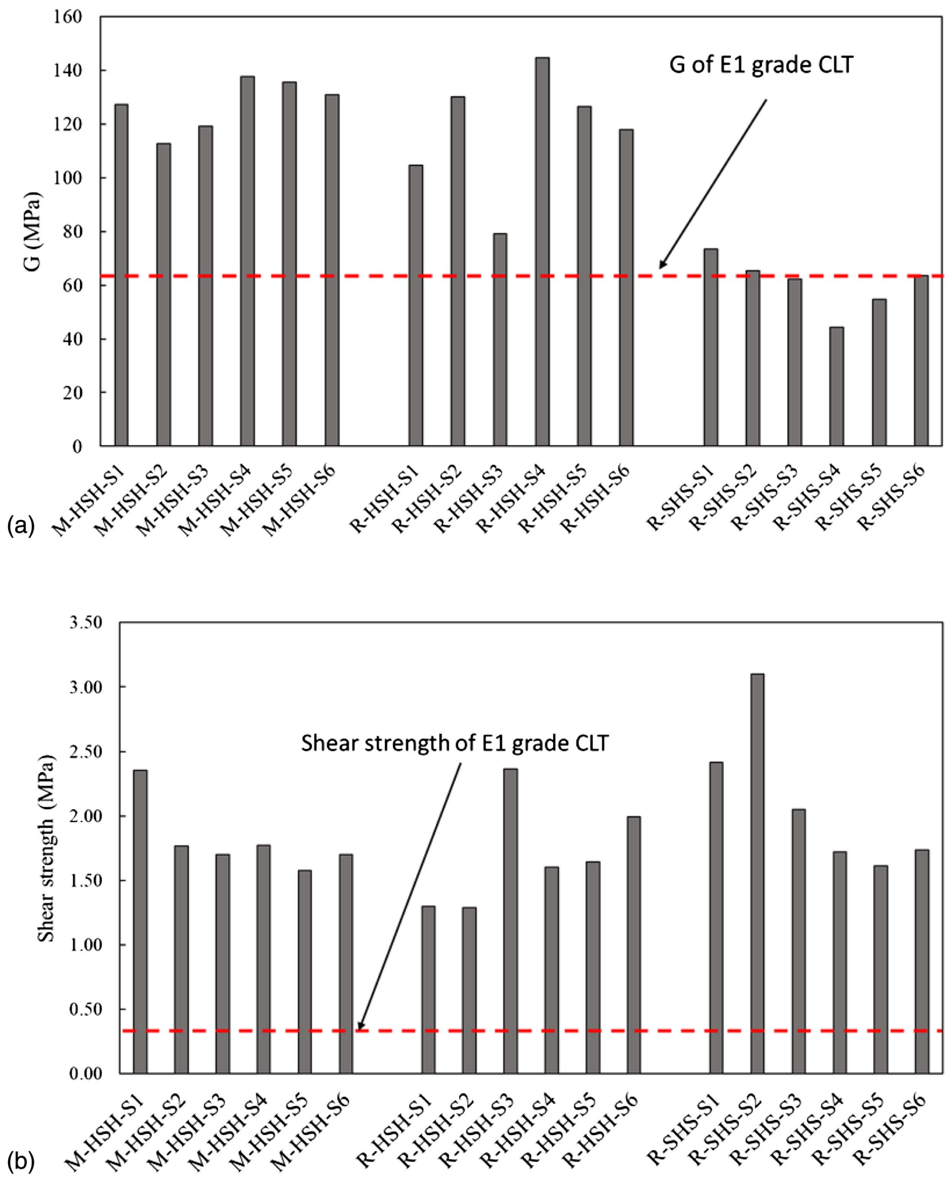

Fig. 7. Reference value in APA/PRG-320 (APA 2019) and the tested value of (a) shear modulus; and (b) shear strength.

study, the input data range for spruce layers ranged from 7,720 to 9,731 MPa, which matched the values from the cited studies. The ν_{12}, ν_{13}, and ν_{23} of the white spruce were 0.467, 0.372, and 0.245, respectively (Ross 2010).

For sugar maple layers, the conversion ratios from MOE_{ND} to elastic modulus in the tangential and radial directions and the shear modulus in the LR and LT directions were 0.065, 0.132, 0.111, and 0.063, respectively. Yellow poplar has a similar specific gravity range and is a diffuse-porous hardwood, as is sugar maple. The conversion ratio to G_{RT} based on the data of yellow poplar is 0.011 (Ross 2010). The average elastic modulus of sugar maple in the longitudinal direction was found to be 13.3 GPa (1.93 Mpsi) by Dickinson et al. (2019), which is close to the measured value. The planar shear modulus (G_{RT}) of similar diffuse-porous hardwoods (white and yellow birch) tested by Gong et al. (2015) varied from 161 to 193 MPa. The input shear modulus value in the RT direction were in the reference value range. The ν_{12}, ν_{13}, and ν_{23} of the maple layers were 0.476, 0.424, and 0.349, respectively.

Damage Model

The progressive damage analysis model is applied to capture the damage of timber (Camanho and Dávila 2002). Timber is considered as an orthogonal material to capture the anisotropic properties. The initiation of damage is detected by the Hashin and Rotem damage criteria in finite-element computation (Barbero et al. 2013). Timber is simulated as a combination of matrix material and fiber in the longitudinal direction. Six parameters are required to define the failure criteria: F_{1t} and F_{2t} are the tensile strengths in the longitudinal direction and transverse direction, respectively; F_{1c} and F_{2c} are the compressive strengths in the longitudinal and transverse directions, respectively; and F_6 and F_4 are the longitudinal shear strength and transverse shear strength, respectively. Four different damage mechanisms are considered in the Hashin damage criteria. The four indexes in the calculation are the tensile index along the fiber direction (F_f^t), the compressive index along the fiber direction (F_f^c), the transverse tensile index (F_m^t), and the transverse compressive index (F_m^c) [Eqs. (9)–(12)]. The damage initiates when any of these indexes exceeds 1.0

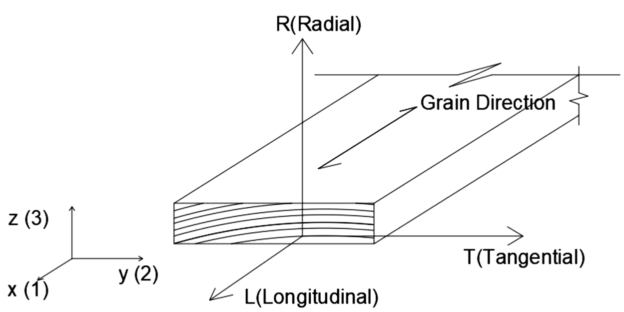

Fig. 8. Definition of timber material model directions.

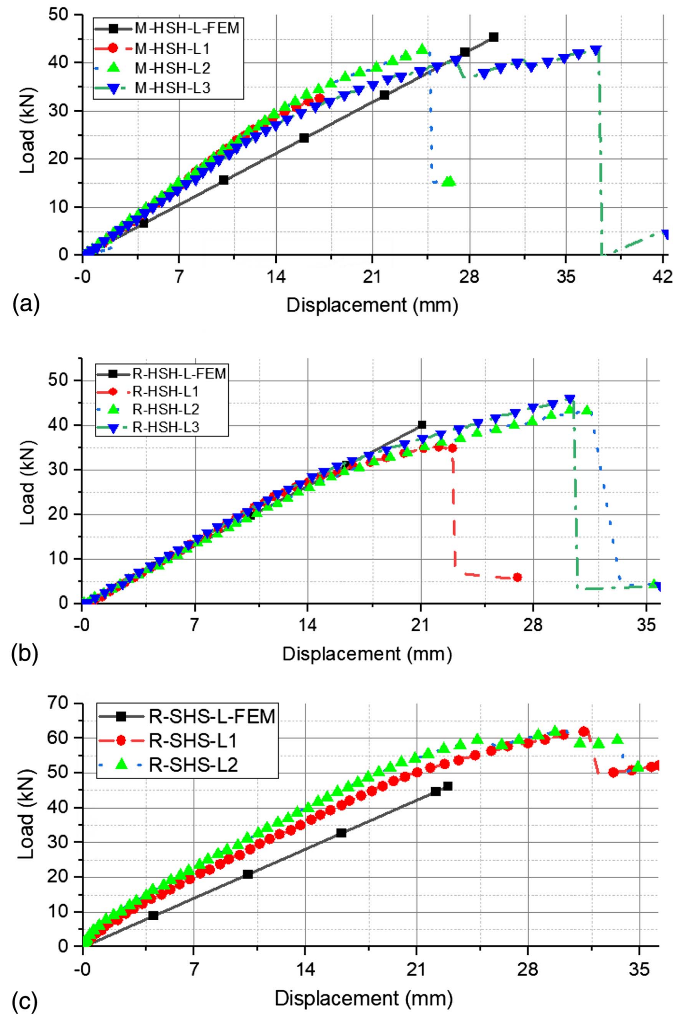

Fig. 9. Long-span third-point bending test load–displacement curves: (a) M-HSH; (b) R-HSH; and (c) R-SHS.

Table 4. Modulus input of CLT beams (MPa)

CLT type	CLT layer	E_1	E_2	E_3	G_{12}	G_{13}	G_{23}
M-HSH	Longitudinal layers	1.66×10^4	1.08×10^3	2.19×10^3	1.84×10^3	1.05×10^3	1.83×10^2
(L1–L3, S1–S6)	Transverse layer	7.72×10^3	4.55×10^2	9.88×10^2	9.57×10^2	9.26×10^2	7.72×10^1
R-HSH	Longitudinal layers	1.67×10^4	1.09×10^3	2.21×10^3	1.86×10^3	1.05×10^3	1.84×10^2
(L1–L3, S1–S6)	Transverse layer	9.30×10^3	5.49×10^2	1.19×10^3	1.15×10^3	1.12×10^3	9.30×10^1
R-SHS	Longitudinal layers	9.73×10^3	5.74×10^2	1.25×10^3	1.21×10^3	1.17×10^3	9.73×10^1
(L1–L3, S1–S6)	Transverse layer	1.52×10^4	9.87×10^2	2.00×10^3	1.68×10^3	9.56×10^2	1.67×10^2

Table 5. Failure criteria of different CLT sample layers (MPa)

Panel type	Layer type	F_{1c}	F_{1t}	F_{2c}	F_{2t}	F_6	F_4
M-HSH(L1–L3, S1–S6)	Longitudinal layers	9.61×10^1	1.43×10^2	1.33×10^1	7.22×10^0	2.09×10^1	4.82×10^0
	Transverse layer	2.80×10^1	5.07×10^1	2.32×10^0	1.94×10^0	5.24×10^0	1.20×10^0
R-HSH(L1–L3, S1–S6)	Longitudinal layers	9.68×10^1	1.44×10^2	1.34×10^1	7.27×10^0	2.11×10^1	4.85×10^0
	Transverse layer	3.37×10^1	6.11×10^1	2.80×10^0	2.34×10^0	6.31×10^0	1.45×10^0
R-SHS(L1–L3, S1–S6)	Longitudinal layers	3.52×10^1	6.40×10^1	2.93×10^0	2.45×10^0	6.60×10^0	1.52×10^0
	Transverse layer	8.78×10^1	1.30×10^2	1.22×10^1	6.59×10^0	1.91×10^1	4.40×10^0

1. Longitudinal tension ($\sigma_{11} \geq 0$)

$$F_f^t = \left(\frac{\sigma_{11}}{F_{1t}}\right)^2 + \alpha\left(\frac{\sigma_{12}}{F_6}\right)^2 \quad (9)$$

2. Longitudinal compression ($\sigma_{11} \leq 0$)

$$F_f^c = \left(\frac{\sigma_{11}}{F_{1c}}\right)^2 \quad (10)$$

3. Transverse tension and/or shear ($\sigma_{22} \geq 0$)

$$F_m^t = \left(\frac{\sigma_{22}}{F_{2t}}\right)^2 + \left(\frac{\sigma_{12}}{F_6}\right)^2 \quad (11)$$

4. Transverse compression ($\sigma_{22} < 0$)

$$F_m^c = \left(\frac{\sigma_{22}}{2F_4}\right)^2 + \left[\left(\frac{F_{2c}}{2F_4}\right)^2 - 1\right]\frac{\sigma_{22}}{F_{2c}} + \left(\frac{\sigma_{12}}{F_6}\right)^2 \quad (12)$$

where σ_{ij} = components of stress tensor; and α = preset parameter defining contribution of shear stress to fiber tensile criterion.

The strengths of the laminations were not tested, because no techniques are available for the nondestructive measurement. The timber strengths were found to be approximately proportional to the MOE (Frühwald and Schickhofer 2005; Guntekin et al. 2014). As a result, the strengths of layers were assumed to be proportional to the reference values. For each layer, the ratio was determined as the ratio of the longitudinal elastic modulus MOE_{ND} (Table 1) to the reference MOE of the layer species from *Wood Handbook* (Ross 2010). The strength of each layer was calculated based on the reference value and the ratio. The input of the timber properties was based on the direction of the layer; F_{1c}, F_{1t}, and F_6 were the compressive, tensile, and shear strengths in the longitudinal direction, and F_{2c}, F_{2t}, and F_4 were the transverse strengths. The strength values are listed in Table 5. The longitudinal compressive strength of sugar maple is 73 MPa (10,587 psi) in a dry condition (Hernández 2007). The longitudinal shear strength of sugar maple averages 15.92 MPa (Okkonen and River 1988). The reference values indicate that the estimated parameters in Table 5 are in a reasonable range.

In the damage model, the fracture energy of each damage pattern is required to capture the occurrence of failure. Fractures are expected to be avoided in all load cases by design in the structural application of CLT panels. However, data on the fracture energy of timber materials are limited. As a result, capturing the postfracture

Table 6. Simulation and test results of long-span beams

Sample type	Peak load (kN)	Peak displacement (mm)	MOE_{CLT} (MPa)	MOE_{CLT} relative difference (%)	MOR_{CLT} (MPa)	MOR_{CLT} relative difference (%)
M-HSH-L	4.53×10^1	2.97×10^1	2.27×10^4	−5.21	4.99×10^1	13.66
R-HSH-L	4.01×10^1	2.10×10^1	2.84×10^4	25.64	4.41×10^1	−4.45
R-SHS-L	4.62×10^1	2.29×10^1	1.87×10^4	14.71	3.72×10^1	−14.89

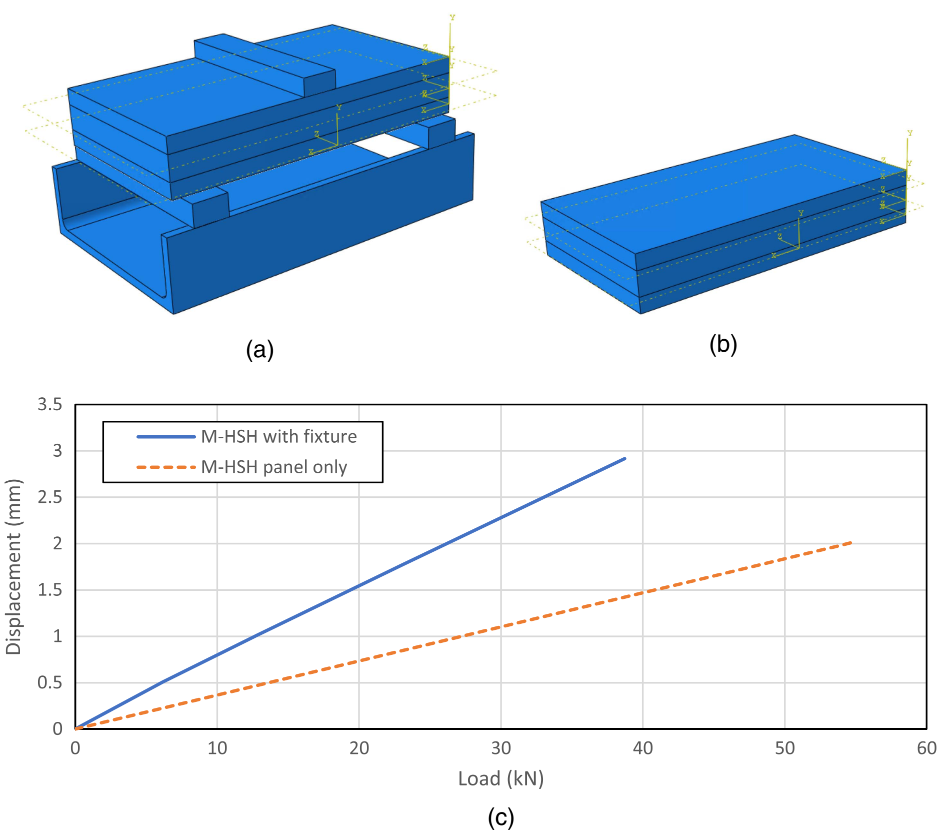

Fig. 10. (a) Model scheme of panel with fixture; (b) model scheme of beam only; and (c) result of short-span model with and without the fixture.

behavior of the panels was not one of the primary objectives. The fracture energy in the damage model was simplified as the conservative value of all directions of the material. The test result of European spruce (*Picea Abies*) in the weakest direction was 485 $N \cdot m/m^2$ (Franke and Quenneville 2014). Because European spruce is close to white spruce, the data can be considered as a conservative assumption to the model parameter. Therefore, the fracture energy was input for the damage model.

Simulation Results and Comparison with Test Data

Long-Span Test Simulation Results

The model was established based on the test setup and sample dimensions (Fig. 1). A displacement-controlled load was applied onto the surface nodes instead of the loading head. The supports were assigned by restraining the nodes at the support locations. The CLT beams were modeled in layers with the model and input with the parameter as in Tables 4 and 5. The simulated load–displacement curves are shown in Fig. 9, along with the correlated test results. The detailed results, including simulated MOE and MOR, are listed in Table 4.

The simulation could not capture the damage accumulation and propagation in the timber (Fig. 9). The models provided a straight line rather than curves with noise and softening. The differences of the key parameters between the results of the modeling and the testing are listed in Table 6. The bending elastic modulus MOE_{CLT} of M-HSH-L was calculated as 2.27×10^4 MPa, which was 5.21% less than the average test result. This indicates that the simulation remained in the range of the test results. The simulation of R-HSH-L is providing an estimated MOE with relatively large difference (25.64%) comparing with other cases. However, the simulation captured the initial tangential modulus [Fig. 9(b)]. Similarly, the R-SHS-L model result was 14.71% larger than the test value. However, the result was in the range of test results (Table 2). Therefore, the R-SHS-L model can be considered acceptable. Overall, the simulation adequately simulated the MOE of long-span CLT beams.

The simulated MOR_{CLT} of M-HSH-L was 13.66% larger than the average test result, which was within the range of test values of the M-HSH-L–type CLT beams. The simulated MOR_{CLT} of R-HSH-L was close to the test value, a relative difference of 4.45%. For R-SHS-L, the simulated MOR_{CLT} was very different from the test result. However, because the minimum of the results was 29.9 MPa, the simulation result was in the range of the test values. Therefore, the simulation can be considered to provide a conservative estimation with reasonable results for the long-span tests.

Short-Span Test Simulation Model Setup

As the first step, the elastic deformation of the fixture was deducted to calibrate the simulation result of the CLT beams. Two metal bars on a channel beam were the supports of the CLT beams in the short-span bending test [Fig. 2(a)]. The total deformation of the fixture was estimated by simulating the models with and without fixtures [Figs. 10(a and b)]. The metal fixtures were simulated for isotropic elastic behavior according to the designed raw material and geometries. The loading heads were made of Type 7000 aluminum alloy with an elastic modulus of 68.95 GPa and a Poisson's ratio of 0.33. The base channel beam and the support bars were made of A36 low-carbon steel. The elastic modulus was 77.91 GPa, and the Poisson's ratio was 0.26. The beam sample layer properties used were those of M-HSH (Tables 5 and 6). The simulated contacts included all the sample-to-fixtures contact and contacts between fixture parts. They were assigned as hard contact in the normal direction,

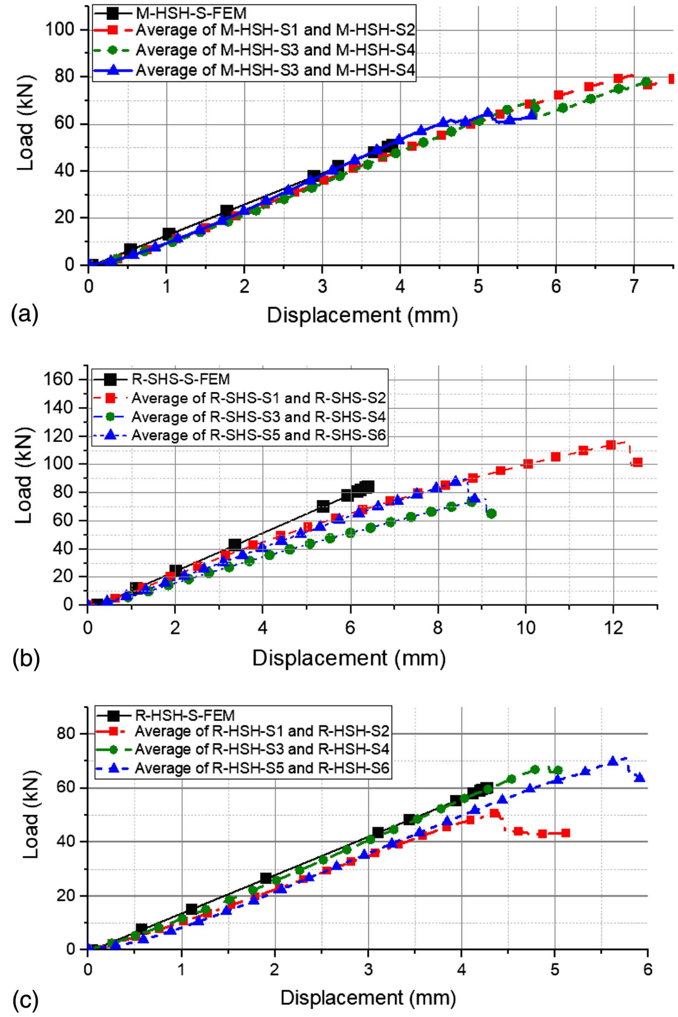

Fig. 11. Tested and simulated short-span bending load–displacement curves of (a) M-HSH; (b) R-HSH; and (c) R-SHS.

and a friction coefficient of 1.0 was assigned in the tangential direction.

The displacement caused by fixture deformation can be estimated as the difference between the results of the two models [Fig. 10(c)]. Because the behavior of the fixture remained elastic during the test, the load–displacement correlation of the fixture can be estimated as linear. According to the results, the deformation was about 0.0381 mm/kN load applied. The load-dependent deformation was used for the model result calibration in the following short-span beam models.

Short-Span Test Simulation Results

Combined with the calibration of the fixture deformation, the total deformation of each sample and fixture were calculated combining the fixture deformation. The load–displacement curves from the test and simulation of each sample type are shown in Figs. 11(a–c). The shear modulus G and the shear strength were calculated based on Eqs. (4)–(6) with the simulated load–displacement curves. The calculated results are listed in Table 7, along with the relative difference from the tested results. The calculated results were compared with the average values of each sample type obtained from tests.

The gradations of the simulated curves were close to the correlated tested curves (Fig. 11). Perhaps due to gradual damage

J. Mater. Civ. Eng., 2021, 33(7): 04021171

Table 7. Simulated mechanical properties of short-span CLT beams and relative differences of tested results

Sample type	Peak load (kN)	Peak displacement (mm)	G (MPa)	G relative difference (%)	Shear strength (MPa)	Shear strength relative difference (%)
M-HSH-S	50.99	3.9	71.30	22.09	1.38	−23.67
R-HSH-S	60.14	4.28	76.65	27.11	1.63	−4.16
R-SHS-S	84.29	4.9	61.30	73.81	1.43	−32.29

accumulation in the spruce layers, the tangential gradation of tested load–displacement curve of the R-SHS-S progressively decreased with the displacement. As a result, the relative difference of the shear modulus between the simulation and tested results was less than 5% for both the M-HSH-S and the R-HSH-S types. For the R-SHS-S type, the simulation provided a gradation with a large difference, which could be the result of overestimation of the timber stiffness. However, the initial tangential modulus was captured by the model, and so the model can be considered adequate for estimation.

The simulated shear strength had a relatively larger difference from the tested result. The difference between the tested and simulated shear strength of M-HSH-S and R-SHS-S was larger than 20% (Table 7). However, due to the large variety of tested results (Table 3), all three simulated results were in or close to the range of tested results. The underestimation might have been the result of the conservative input parameters. The result can be considered as a conservative estimation to the actual shear strength.

It can be concluded that the model can provide a general estimation or prediction of the mechanical properties, including MOE, MOR, shear modulus, and shear strength. The accuracy of the model is not sufficient to provide specific sample-to-sample simulation, because it does not include the variance of timber properties and local defects. However, the model can adequately estimate the mechanical properties based on lamination longitudinal elastic modulus and related reference values of the corresponding CLT layup. Therefore, the models are efficient tools for predicting the mechanical properties of CLT beams with a hybrid layup of softwood and hardwood.

Conclusions

Hybrid CLT made with low-value sugar maple and white spruce was designed to promote the market for low-value sugar maple, which is limited to used in low-value-added products. The developed hybrid CLT can enhance forest management and benefit the environment. The studied CLT panels included two hybrid layups of sugar maple and white spruce along with two common adhesives. The mechanical properties of hybrid CLT panels were tested with long-span and short-span flexural tests and simulated in both cases. The following conclusions were drawn:

1. The adhesive type did not have a significant impact on the elastic modulus and bending strength of the CLT beams. The layup with sugar maple longitudinal layers had significantly higher bending elastic modulus and bending strength. The sugar maple transverse layer enhanced the shear strength of the panel.
2. Melamine provided a better shear modulus and slightly higher shear strength than did resorcinol. The R-SHS–type CLT had much higher shear strength than the R-HSH–type CLT, indicating that a strong transverse layer can more effectively enhance the shear strength of CLT than can strong longitudinal layers.
3. Compared with current standard E1-type CLT (PRG-320), the bending modulus, bending strength, shear modulus, and shear strength all were enhanced when using hardwood longitudinal layers. The hardwood transverse layer enhanced the MOE and MOR were similarly, and the shear strength was improved to a greater degree. The shear modulus, however, was found to be the same or less than that of the E1 CLT. All three hybrid CLT types fulfilled the mechanical property requirements of PRG-320.
4. The FE model can approximately capture the elastic modulus, shear modulus, modulus of rupture, and shear strength of each CLT type in the long-span and short-span bending tests based on the lamination elastic modulus and different layups. Although the accuracy of the model was not sufficient to provide a specific sample-to-sample simulation, the model can adequately estimate the performance of each CLT-type based on limited information of the laminations used.

In summary, the results of this study suggested that the hybrid CLT with low-value sugar maple and white spruce can provide better structural performance than standard CLT made with spruce-pine-fir. Enhancing the panel properties by using low-value sugar maple lumber in individual layers is feasible and effective. Using the finite-element model to estimate the mechanical properties of the hybrid CLT panels based on the lamination properties can help to examine the layup design of mixed-species hybrid CLT.

Data Availability Statement

All data, models, and code generated or used during the study appear in the published article.

Acknowledgments

This study was partially supported through a cooperative research agreement (FS 17-JV-11111133-034) between Michigan Technological University and the USDA Forest Service Forest Products Laboratory. The authors are grateful to AJD Forest Products (Grayling, Michigan) for donating the low-value sugar maple lumber for this project.

References

APA (The Engineered Wood Association). 2011. *Standard for performance-rated cross laminated timber*. ANSI/APA PRG 320. Washington, DC: APA.

APA (The Engineered Wood Association). 2019. *Standard for performance-rated cross laminated timber*. ANSI/APA PRG-320-2019. Washington, DC: APA.

ASTM. 2011. *Standard practice for estimating the percentage of wood failure in adhesive bonded joints*. ASTM D5266-99. West Conshohocken, PA: ASTM.

ASTM. 2012. *Standard test methods for nondestructive evaluation of wood-based flexural members using transverse vibrations*. ASTM D6874-12. West Conshohocken, PA: ASTM.

ASTM. 2013. *Standard test method for strength properties of adhesive bonds in shear by compression loading*. ASTM D905-08. West Conshohocken, PA: ASTM.

ASTM. 2015. *Standard test methods of static tests of lumber in structural sizes.* ASTM D198. West Conshohocken, PA: ASTM.

Barbero, E. J., F. A. Cosso, R. Roman, and T. L. Weadon. 2013. "Determination of material parameters for Abaqus progressive damage analysis of E-glass epoxy laminates." *Composites, Part B: Eng.* 46: 211–220. https://doi.org/10.1016/j.compositesb.2012.09.069.

Beaulieu, J., S. Y. Zhang, Q. Yu, and A. Rainville. 2007. "Comparison between genetic and environmental influences on lumber bending properties in young white spruce." *Wood Fiber Sci.* 38 (3): 553–564.

Bendtsen, B. A. 1974. *Specific gravity and mechanical properties of black, red, and white spruce and balsam fir*. Madison, WI: Dept. of Agriculture, Forest Service, Forest Products Laboratory.

Brandner, R. 2013. *Stochastic system actions and effects in engineered timber products and structures.* Graz, Austria: Verlag der Technischen Universität Graz.

Brank, B., A. Stanić, M. Lavrenčič, and B. Hudobivnik. 2017. "Design optimization and failure modelling of ribbed cross-laminated timber plates." In Vol. 4 of *Proc., 11th Int. Conf. Shell Structures: Theory and Applications (SSTA 2017), October 11–13*, 69. Boca Raton, FL: CRC Press.

Camanho, P. P., and C. G. Dávila. 2002. *Mixed-mode decohesion finite elements for the simulation of delamination in composite materials.* NASA/TM-2002-211737. Hampton, VI: National Aeronautics and Space Administration.

Chen, Y., and F. Lam. 2012. "Bending performance of box-based cross-laminated timber systems." *J. Struct. Eng.* 139 (12): 04013006. https://doi.org/10.1061/%28ASCE%29ST.1943-541X.0000786.

Dickinson, Y., X. Wang, J. Wiedenbeck, and R. J. Ross. 2019. *Effects of silviculture practices on engineering properties of northern hardwood species of the Great Lakes Region: A literature review.* General Technical Rep. FPL-GTR-269. Madison, WI: US Dept. of Agriculture, Forest Service, Forest Products Laboratory.

Flores, E. I. S., K. Saavedra, J. Hinojosa, Y. Chandra, and R. Das. 2016. "Multi-scale modelling of rolling shear failure in cross-laminated timber structures by homogenisation and cohesive zone models." *Int. J. Solids Struct.* 81: 219–232. https://doi.org/10.1016/j.ijsolstr.2015.11.027.

Franke, B., and P. Quenneville. 2014. "Analysis of the fracture behavior of Radiata Pine timber and Laminated Veneer Lumber." *Eng. Fract. Mech. Eng. Fract. Mech.* 116: 1–12. https://doi.org/10.1016/j.engfracmech.2013.12.004.

Frühwald, K., and G. Schickhofer. 2005. "Strength grading of hardwoods." In *Proc., 14th Int. Symp. on Nondestructive Testing of Wood*, 199–210. Madison, WI: Structural Building Components Association.

Gharib, M., A. Hassanieh, H. Valipour, and M. A. Bradford. 2017. "Three-dimensional constitutive modelling of arbitrarily orientated timber based on continuum damage mechanics." *Finite Elem. Anal. Des.* 135: 79–90. https://doi.org/10.1016/j.finel.2017.07.008.

Gong, M., D. Tu, L. Li, and Y. Chui. 2015. "Planar shear properties of hardwood cross layer in hybrid cross laminated timber." In *Proc., ISCHP 2015* 85–90. Pointe-Claire, QC: FPInnovations.

Guntekin, E., S. Ozkan, and T. Yilmaz. 2014. "Prediction of bending properties for beech lumber using stress wave method." *Maderas Cienc. Tecnol.* 16 (1): 93–98.

Hashin, Z., and A. Rotem. 1973. "A fatigue failure criterion for fiber reinforced materials." *J. Compos. Mater.* 7 (4): 448–464. https://doi.org/10.1177/002199837300700404.

He, M., X. Sun, and Z. Li. 2018. "Bending and compressive properties of cross-laminated timber (CLT) panels made from Canadian hemlock." *Constr. Build. Mater.* 185: 175–183. https://doi.org/10.1016/j.conbuildmat.2018.07.072.

Hernández, R. E. 2007. "Influence of accessory substances, wood density and interlocked grain on the compressive properties of hardwoods." *Wood Sci. Technol.* 41 (3): 249. https://doi.org/10.1007/s00226-006-0114-5.

Hindman, D. P., and J. C. Bouldin. 2015. "Mechanical properties of southern pine cross-laminated timber." *J. Mater. Civ. Eng.* 27 (9): 04014251. https://doi.org/10.1061/(ASCE)MT.1943-5533.0001203.

Karacabeyli, E., and B. Douglas. 2013. *CLT handbook: Cross-laminated timber*. Point-Claire, QC: FPInnovations.

Khasa, P. D., and B. P. Dancik. 1996. "Rapid identification of white-Engelmann spruce species by RAPD markers." *Theor. Appl. Genet.* 92 (1): 46–52. https://doi.org/10.1007/BF00222950.

Lu, W., J. Gu, and B. Wang. 2019. "Study on flexural behavior of cross-laminated timber based on different tree species." *Adv. Mater. Sci. Eng.* 2019. https://doi.org/10.1155/2019/1728258.

Musah, M. 2020. "Bonding hardwood lumber for cross laminated timber: Properties and environmental impacts." Ph.D. thesis, College of Forest Resources and Environmental Science, Michigan Technological Univ.

Navaratnam, S., P. B. Christopher, T. Ngo, and T. V. Le. 2020. "Bending and shear performance of Australian Radiata pine cross-laminated timber." *Constr. Build. Mater.* 232: 117215. https://doi.org/10.1016/j.conbuildmat.2019.117215.

NHLA (National Hardwood Lumber Association). 2019. *Rules for the measurement & inspection of hardwood and cypress*. Memphis, TN: NHLA.

Okkonen, E. A., and B. H. River. 1988. "Factors affecting the strength of block-shear specimens." *For. Prod. J.* 39 (1): 43–50.

Ross, R. J. 2010. *Wood handbook: Wood as an engineering material.* General Technical Rep. FPL-GTR-190. Madison, WI: USDA Forest Service, Forest Products Laboratory.

Sharifnia, H., and D. P. Hindman. 2017. "Effect of manufacturing parameters on mechanical properties of southern yellow pine cross laminated timbers." *Constr. Build. Mater.* 156: 314–320. https://doi.org/10.1016/j.conbuildmat.2017.08.122.

Shivnaraine, C. S., and I. Smith. 1990. "Influence of juvenile wood on bending properties of softwood lumber." *J. Forest Eng.* 1 (2): 25–33. https://doi.org/10.1080/08435243.1990.10702616.

Sun, X., M. He, and Z. Li. 2020. "Novel engineered wood and bamboo composites for structural applications: State-of-art of manufacturing technology and mechanical performance evaluation." *Constr. Build. Mater.* 249: 118751. https://doi.org/10.1016/j.conbuildmat.2020.118751.

Thomas, R. E., and U. Buehlmann. 2017. "Using low-grade hardwoods for CLT production: a yield analysis." In *Proc., 6th Int. Scientific Conf. on Hardwood Processings*, edited by V. Möttönen and E. Heinonen, 199–206. Helsinki, Findland: Natural Resources Institute of Finland.

Wang, Z., H. Fu, Y.-H. Chui, and M. Gong. 2014. "Feasibility of using poplar as cross layer to fabricate cross-laminated timber." In *Proc., World Conf. on Timber Engineering*. Quebec City: World Conference of Timber Engineering.

Zhou, H., and I. Smith. 2007. "Factors influencing bending properties of white spruce lumber." *Wood Fiber Sci.* 23 (4): 483–500.